Biomaterials

CrossMark

Tungsten film as a hard and compatible carrier for antibacterial agent of silver

L. J. Wang[1], F. Zhang[1], A. Fong[2], K. M. Lai[2], P. W. Shum[2], Z. F. Zhou[3], T. Fu[1,*] (iD), P. Ning[1], and S. Y. Yang[1]

[1] *Key Laboratory of Biomedical Information Engineering of Ministry of Education, School of Life Science and Technology, Xi'an Jiaotong University, Xi'an 710049, China*
[2] *Asahi Group Co. Ltd, Kwun Tong, Hong Kong, China*
[3] *Department of Mechanical and Biomedical Engineering, City University of Hong Kong, Kowloon, Hong Kong, China*

ABSTRACT

Silver-containing tungsten (W–Ag) films for antibacterial applications were deposited on glass, silicon, and 316L stainless-steel substrates by magnetron sputtering with the silver target current of 0–2.0 A. The addition of silver improves adhesion of the films on glass substrate due to the reduced residual stress in the films. SEM and EDX analyses reveal Ag-rich tiny dots ($\sim$ 20 nm) at the surface of W–Ag films with high silver contents. In XRD patterns, silver peaks are present for the samples deposited at 1.5 and 2.0 A, and tungsten grain size is decreased from $\sim$ 23 to 10 nm by silver addition. XPS analysis shows that tungsten is slightly oxidized (WO_3) at the top surface of the film, and silver presents mainly in metallic state. The low Ag/W ratios and the small surface roughness ($<$ 8 nm) indicate that silver segregation at the film surface is not obvious. Microhardness of the samples with $\leq$ 6.7 at.% silver is nearly seven times that of the stainless steel ($\sim$ 250 HV). The coated samples are hydrophobic tested by contact angle measurement. The potentiodynamic polarization and the soaking test simulating the inflammatory state show that even corrosion occurs and silver addition decreases corrosion resistance of the films. The antibacterial ratio of the coated samples increases with silver content, being 91% at 4.2 at.% silver content tested by agar plate counting method. In agar disk diffusion assay, no inhibition zone is observed for all samples. The antibacterial property of the W–Ag films is localized, long-lasting, and reusable, which would be beneficial for their potential biomedical and environmental applications.

Address correspondence to E-mail: taofu@xjtu.edu.cn

Introduction

The hospital-acquired infections (HAIs) continue to be a major public health concern in hospitals and healthcare units worldwide. It has been reported that HAIs, of which a large portion are derived by contact transmission, are ranked in the top 10 causes of death in the USA, and there are 300,000 cases of HAIs annually in the UK leading to 5000 deaths and over £3 billion loss to the National Health Service [1, 2]. It is of great importance to reduce the spread of unwanted bacteria in clinical and environmental applications.

More than 20 metallic elements have been investigated for bactericidal property, including Ag, Cu, Zn, W, Mn, Al, Si, Ti, V, Cr, Co, Ni, Zr, Nb, Mo, Pd, Sn, Ta, Pb, Au, and Pt [3]. Among them, silver has been known as an effective and long-term antimicrobial agent since the ancient times, with the broad spectrum against multiple drug-resistant bacteria and the limited toxicity toward mammalian cells [4–6]. The biocompatible elements such as Cu, Zn, W, Mn, Ta were also reported to possess antimicrobial activity [3, 7].

Silver has been added into vapor-deposited ceramic coatings to produce a hard, wear-resistant, and antibacterial surface layer on different substrates, e.g., ZrNO–Ag [8], TaN-(Ag,Cu) [9], TiN–Ag [10], and diamond-like carbon (DLC)–Ag films [11, 12]. Silver segregation from ceramic films due to their different nature was observed during the deposition and the aging in ambient or wet conditions [12, 13]. The segregation of silver to film surface will increase the biocompatibility concern of silver, and the nano-sized voids left in the films may impair corrosion resistance of the composite films.

Silver-containing metallic films were also prepared for antibacterial applications. For example, the Ti–Ag film with ~ 70 at.% Ag was composed of Ti$_3$Ag and Ag phases, and the surface was smooth and devoid of silver particles [14]. The Ti–Ag films with < 21.6 at.% Ag exhibited solid solution structure [15]. The Nb–Ag film with ~ 50 at.% Ag contained crystalline silver, and the surface was covered with Ag agglomerates [14]. Structural evolution of the films with silver content is interesting for antibacterial films, for silver content together with its distribution plays crucial roles in silver ions release and thus antibacterial activity of the films. For mechanical properties, the

Ag-containing metallic films normally have lower hardness (e.g., 2–8 GPa for Ti–Ag films [16]) and weaker wear resistance than the ceramic films (e.g., 13.3 GPa for DLC film [12], 12.5–15.4 GPa for TaN-(Ag,Cu) films [9]).

Tungsten is a well-known metal for its high hardness, high melting point, and good resistance to air erosion at room temperature. Tungsten is widely utilized in different industrial fields, and the vapor-deposited W or W-containing films are hard (14.1–32.3 GPa for W films [17–19]) and well biocompatible [20–22]. It was also found that W-containing DLC film inhibited the growth of some bacteria strains, and it significantly reduced biofilm formation [7]. The potential biomedical applications of W and W-based films are needed to be explored.

Tungsten film would provide a hard, wear-resistant, structurally compatible, and biocompatible matrix to carry silver and other antibacterial agents. In this work, silver-containing tungsten (W–Ag) films with up to 36.2 at.% Ag are deposited by magnetron sputtering, and microstructure, composition, microhardness, wettability, corrosion resistance, and antibacterial activity of the coated samples are investigated for their potential biomedical and environmental antibacterial applications.

Experimental

Samples preparation

The W–Ag films were deposited on glass slides, silicon wafers, and 316L stainless-steel disks (ϕ 10 × 1 mm^2) by an industrial-scale magnetron sputtering system. The substrates were degreased, ultrasonically cleaned, and subsequently blown dry in flowing nitrogen gas. In the sputtering system, one tungsten target and one silver target (purity > 99.9%) were fixed for the deposition. The substrates were mounted on the substrate holder (rotating speed 10 rpm), and the target-to-substrate distance was 17 cm. Prior to deposition, the vacuum chamber was evacuated to a background pressure of 9×10^{-4} Pa. Then, pure Ar working gas (99.999% purity) was introduced into the chamber, corresponding to a working gas pressure of 0.24 Pa. For plasma ion etching, the substrates were biased with pulse DC at a frequency of 250 kHz and a voltage of -450 V. During deposition, the substrates were biased at

− 80 V, the tungsten target current was 4.0 A, the silver target current was 0–2.0 A, and the deposition time was 25–50 min. Pure silver film was also prepared for comparison. The samples with slide glass, silicon wafer, and stainless-steel substrate were noted as G, S, and M group samples, respectively (Table 1).

Material characterization and tests

Surface morphology of the coated samples was observed by scanning electron microscopy (SEM, FEI Quanta 600F) equipped with energy-dispersive X-ray analysis (EDX) and atomic force microscopy (AFM, Veeco diInnova, tapping mode). Phase structure of the coated samples was analyzed by X-ray diffraction (XRD, X'Pert PRO, CuK_{α}). Elemental composition and chemical bonding state of the samples were examined by X-ray photoelectron spectroscopy (XPS, VG K-Alpha, AlK_{α}). The spectra were acquired without and with 30 s of ion sputtering to remove surface contaminants. For the sputtering, the angle, current, and energy of the Ar^+ ion gun was 30°, 10 mA, and 2 keV, respectively.

Thickness of the films was obtained by measuring the step height with a stylus surface profiler (Bruker DektakXT, vertical resolution 0.1 nm, stylus radius 5 μm). Surface roughness of the coating samples was assessed by an optical profiler (Veeco Wyko NT9300, vertical resolution < 0.1 nm).

Microhardness of the coatings was measured by Fischerscope HM2000 (Vicker's diamond pyramid indenter, test load 10 mN). Wettability of the samples was assessed by measuring water and glycol contact angles using a contact angle goniometer under ambient conditions. Surface energy of the samples was determined from the above contact angles with

the method based on Owens–Wendt theoretical model [23].

Corrosion resistance of the stainless-steel group samples was evaluated by potentiodynamic polarization test with an electrochemical workstation (Corrtest CS150) under ambient conditions. The electrolyte was a Ca-free Hank's balanced salt solution (HBSS, NaCl 8.00, KCl 0.40, $NaHCO_3$ 0.34, KH_2PO_4 0.06, $Na_2HPO_4 \cdot 12H_2O$ 0.12 g/L), and the counter electrode and reference electrode were platinum electrode and saturated calomel electrode (SCE), respectively. Corrosion resistance of the coated stainless-steel samples was also tested by soaking treatment using acidic phosphate buffer saline (PBS), which simulated the inflammatory state around the implants (NaCl 8.00, KCl 0.20, $Na_2HPO_4 \cdot 12H_2O$ 2.87, KH_2PO_4 0.27 g/L, 30% H_2O_2 1.5 mL/L, pH being adjusted to 5.2 ± 0.1 by 0.4 M HCl [24]). The solution was renewed every 3 days. After 6 days of soaking, the samples were evacuated, washed gently with deionized water, and observed with SEM.

Antibacterial test

Antibacterial property of the samples was assessed by the quantitative evaluation using agar plate counting method and the qualitative evaluation using agar disk diffusion assay against E. Coli, a typical kind of Gram-negative bacteria. *E. coli* has been found in biomaterial-related infection sites and is one of the main sources responsible for hospital-acquired infections. For agar plate counting method, 10 μL of *E. coli* suspension in the concentration of 10^5 colony-forming units (CFU)/mL was dropped onto the sample surface and then covered quickly by a filter membrane. After placed in dark at room temperature

Table 1 Ag target current, deposition time, thickness, roughness, Ag content, and microhardness of the samples

Sample	I_{Ag} (A)	Time (min)	Thick (μm)*	Ra (nm)*	Ag ratio (at.%)+	$HV_{0.001}$*
SS	N.A.	N.A.	N.A.	/	/	/
G/S/M00	0	50	0.38	4.3	0	2100
G/S/M02	0.2	45	0.38	7.7	0.1	1860
G/S/M04	0.4	40	0.39	3.0	2.3	1780
G/S/M06	0.6	40	0.40	6.7	4.2	1750
G/S08	0.8	40	0.42	2.8	6.7	1740
G/S10	1.0	35	0.44	4.2	10.3	1420
G/S15	1.5	30	0.60	4.1	23.9	650
G/S20	2.0	25	0.78	3.6	36.2	570
G/S/MAg	2.0	30	0.74	8.1	100	240

NA not applied, / not tested, *,+ for samples with silicon and glass substrate, respectively

for 3 h, the samples were rinsed with 3 mL of sterilized water to collect the survival bacteria. After stirring, 700 µL of the suspension was spread on Maconkey agar plate evenly using a sterile spreader. The inoculums were incubated aerobically at 37 °C for 24 h. The images of colonies were taken by a digital camera. Each sample was tested triply in one test cycle. In order to study the antibacterial mechanism of W–Ag films, E. coli was cultured on sample M06 and stainless-steel substrate for 3 h and then treated for SEM observation.

For agar disk diffusion assay, E. coli suspension (10^5 CFU/mL) was dropped onto Luria–Bertani agar plate and spread evenly using a sterile spreader. The sterilized samples were placed face down on the inoculated agar plates, with effective contact between them. The seeded agar plates were incubated aerobically at 37 °C for 48 h. The images of the inhibition zone were taken by a digital camera.

Results and discussion

Films characterization

The W–Ag and pure Ag films on stainless-steel substrate (samples M00–M06 and MAg, Fig. 1) and those on silicon substrate (samples S00–S20, SAg) are adherent and smooth. The films on glass substrate are adherent and smooth for samples G06–G20 and GAg, but the samples deposited at low silver target currents (G00–G04) are rough due to peeling off and cracking of the films. Thus, the addition of silver has reduced residual stress in the sputter-deposited tungsten film. The film thickness measured with the
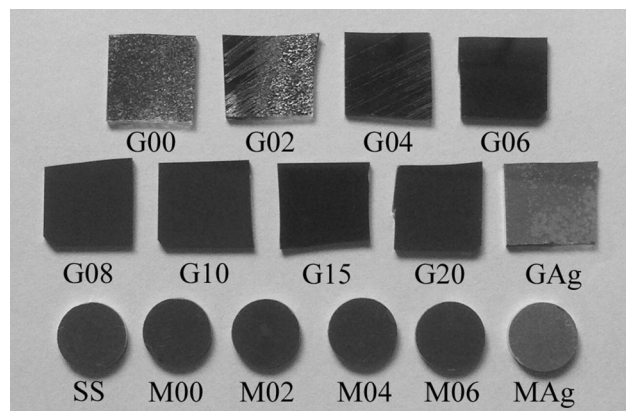

Figure 1 Optical photographs of the samples with glass and stainless-steel substrates.

surface profiler increases with the silver target current (Table 1), ranging from 0.38 µm for sample S00 to 0.78 µm for sample S20. Silver film has a much higher deposition rate (SAg, 24.7 nm/min) than tungsten film (S00, 7.6 nm/min).

SEM surface images of the W–Ag and pure Ag-coated samples are shown in Fig. 2. Similar fine particles with the size of 100–200 nm are observed for the W–Ag films, and the particles are larger (200–400 nm) for pure Ag film. Tiny white dots ($\sim$ 20 nm) are scattered at the surface of W–Ag films deposited at high silver target currents. The higher Ag/W ratios of these dots compared with that of the whole film indicate that they are silver or its oxide nanoparticles. The Ag content of the films obtained by areal EDX analysis increases with the silver target current, e.g., being 4.2, 10.3, 23.9, and 36.2 at.% for G06, G10, G15, and G20, respectively (Table 1).

AFM surface images of the coated glass samples are shown in Fig. 3. Spherical nanoparticles with the size of 110–180 nm are observed for sample G06. Smaller particles (40–100 nm) and big aggregations appear at the surface of samples G15 and G20. Sample GAg has larger particle size and higher surface roughness (Ra = 8.78 nm) than samples G06, G15, and G20 (Ra = 2.24, 5.85, 6.72 nm, respectively).

The surface roughness of W–Ag-coated silicon samples is Ra = 3–8 nm measured by the optical profiler (Table 1). In DLC–Ag films, silver segregation from the carbon matrix is serious [25, 26], and a very rough surface layer (Ra = 21.3 nm) was formed at the silver target current of 0.6 A [12]. The silver segregation-induced roughness increase observed in DLC–Ag films is not obvious for the W–Ag films, which may indicate a different microstructure of the W–Ag films.

In XRD patterns, diffraction peaks from the steel substrate and the tungsten films are present for samples M00–M06 (α-W, ICDD #04-0806), while the silver peaks are absent (Fig. 4a). For the coated glass samples, silver peaks are not detected for G00–G10 (Fig. 4b). A small peak appears at $2\theta = 38.1°$ for sample G15, and there is a shoulder peak at $2\theta = 38.1°$ for sample G20. The two peaks can be ascribed to Ag(111) plane (ICDD #04-0783). The Ag(111) peaks are rather weak for samples G15 and G20 that have the highest silver content, being 23.9 and 36.2 at.%, respectively. Tungsten and silver were reported to be immiscible due to the large positive enthalpy of mixing Ag and W [27], but they have
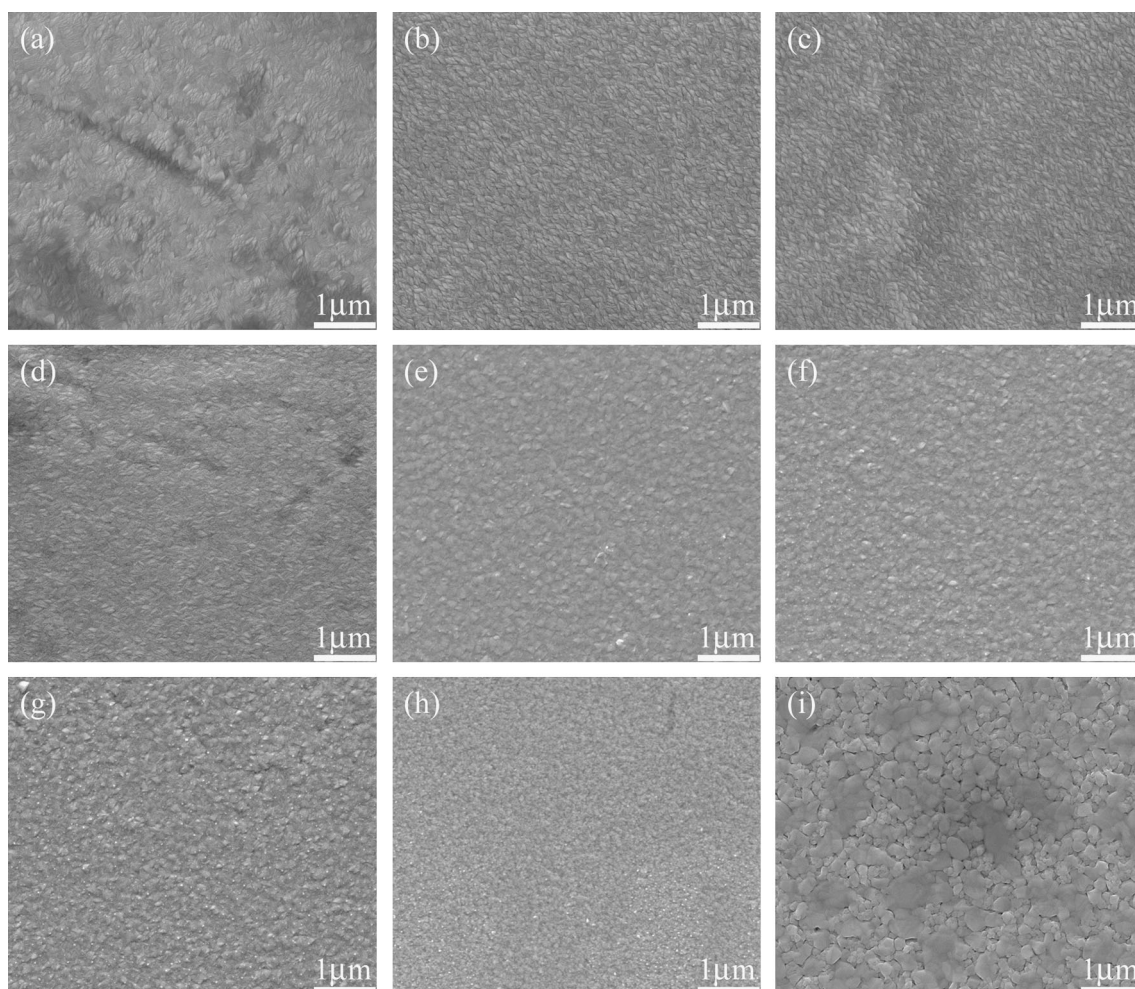
Figure 2 SEM surface images of the W–Ag and the Ag-coated samples: **a** M00, **b** M02, **c** M04, **d** M06, **e** G08, **f** G10, **g** G15, **h** G20, **i** GAg.

similar atomic radius (130 pm for W, 134 pm for Ag). The main diffraction peak can be indexed as W(110) plane by the ICDD file of #04-0806. This peak is positioned at slightly lower 2θ values (39.8°–40.0°) for Ag-containing W films than that for the pure W film (40.1°). It is presumed that silver exists in the tungsten films mainly as solid solution atoms, and the energetic ion bombardment helps form such a metastable crystal structure during film growth. According to the Debye–Scherrer equation, the tungsten grain size is calculated to be 23, 26, 21, 24, 23, 15, 13, and 10 nm for samples G00–G20, respectively, from the diffraction peaks located at $2\theta \approx 39.9°$ and $2\theta = 35.5°$. In particular, additional diffraction peaks are detected for sample G02, which can be indexed with the ICDD file of #47-1319 (β-W [28]) or the file of #65-6453 (α-W [18]). The formation mechanism of the additional peaks needs a further study.

Surface elemental composition of sample G06 was examined by XPS analysis, with the high-resolution W 4f and Ag 3d spectra shown in Fig. 5. Strong W 4f doublets positioned at 37.9 eV ($4f_{5/2}$) and 35.8 eV ($4f_{7/2}$) are indicative of oxidation of tungsten (WO_3) at the top surface of the film. The doublets ascribed to metallic tungsten (31.1/31.2 eV, $4f_{5/2}$; and 33.3 eV, $4f_{7/2}$) are increased, and those of WO_3 are decreased after 30-s sputter etching. In Ag 3d spectra, the doublets are located at 374.1 eV ($3d_{3/2}$) and 368.1 eV ($3d_{5/2}$), respectively. The Ag $3d_{5/2}$ peak for metallic silver is located at higher binding energy (368.4 eV) than those for its oxides (367.8 eV for Ag_2O, 367.4 eV for AgO) [29]. This indicates that silver presents mainly in metallic state, but it is slightly oxidized at the topmost surface when exposed to ambient air. The nonpassive silver oxide thin film is essential for the release of antimicrobial Ag^+ ions in solutions [30, 31].
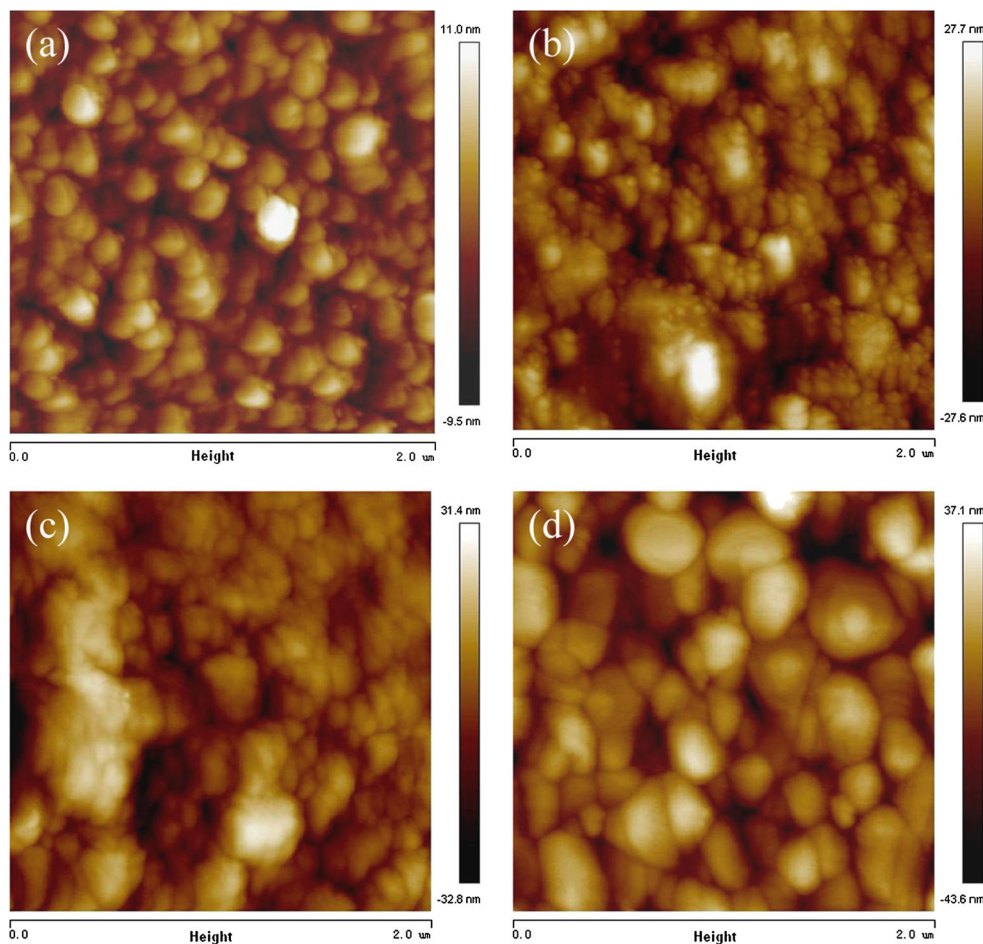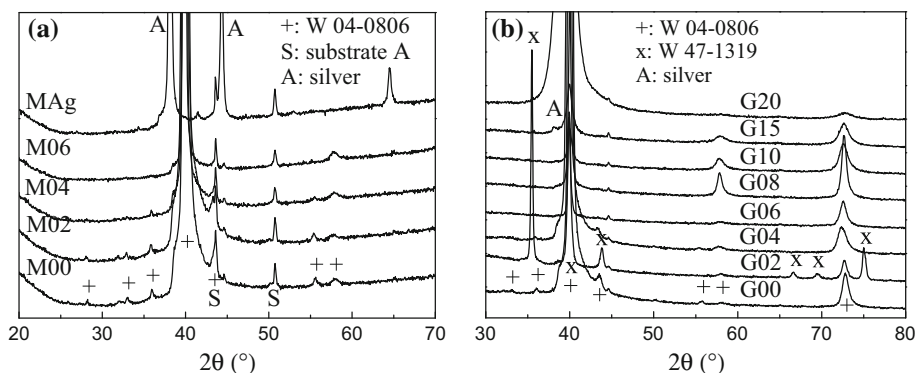
Figure 3 AFM images of the coated glass samples: **a** G06, **b** G15, **c** G20, **d** GAg.

Figure 4 XRD patterns of **a** stainless-steel and **b** glass group samples, in which the W peaks are indexed by the ICDD files of #04-0806 and #47-1319.

The atomic ratio of Ag/W is calculated to be 4.3 and 2.6% before and after 30 s of sputtering, respectively. In comparison, much higher Ag/C ratio (260 at.%) was obtained for DLC–Ag film that was deposited at the same silver target current (0.6 A) [12], which is due to the serious segregation of silver from carbon matrix during and after film deposition [23, 25, 32]. Silver has low solubility with carbon, and it has no ability to form Ag–C compounds [33]. The low Ag/W ratios measured by XPS show that silver segregation at the film surface is not obvious for W–Ag films, agreeing with the above morphology and roughness analyses. Silver exists in the tungsten films mainly as solid solution atoms according to the XRD analysis.

Figure 5 XPS high-resolution W 4*f* and Ag 3*d* spectra of sample G06 before and after 30 s of sputter etching.
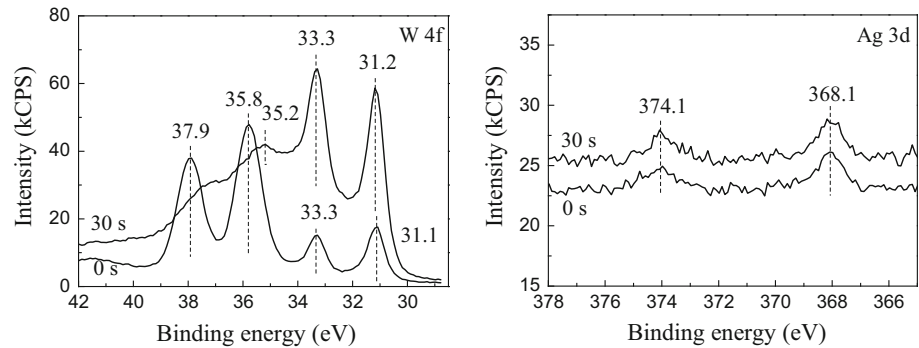

Table 2 Antibacterial agents and the microstructures of the antibacterial agent-containing metallic films or compounds

Element	Lattice type	Atomic radius (pm)	Antibacterial agent/film microstructure
Ag	fcc	134	Antibacterial agent [3, 12]
Cu	fcc	117	Antibacterial agent [3, 9]
Zn	hcp	125	Antibacterial agent [7]
Mn	bcc	117	Antibacterial agent [7]
W	bcc	130	Antibacterial agent [7]
			Solid solution, < 23.9 at.% Ag, and silver segregation at higher content, present work
Nb	bcc	134	Segregation, ∼ 50 at.% Ag [14]
Mo	bcc	130	Solid solution of Mo–Ag [34]
Fe	bcc	117	Solid solution of Fe–Ag [35]
			Fe_2Ag_3, in ICDD
Ti	hcp	132	Solid solution, < 21.6 at.% Ag [15]
			Ti_2Ag, TiAg, Ag/Ti = 0.36 [16]
			Ti_3Ag, TiAg, in ICDD
			Ti_3Ag + Ag, ∼ 70 at.% Ag [14]
Zr	hcp	145	Zr_3Ag, Zr_2Ag, ZrAg, in ICDD
Co	hcp	116	Segregation of Ag nanoparticles [36]

Different microstructures have been reported for vapor-deposited silver-containing metallic films (Table 2). (1) Intermetallic compounds. For sputter-deposited Ti–Ag films, Ti_3Ag was formed in the film at the silver content of ∼ 70 at.% [14]. The phases of Ti_2Ag and TiAg were detected for the heat-treated Ti–Ag films with the Ag/Ti ratio of 0.36 [16]. Fe and Zr can also form compounds with silver according to ICDD files (Table 2). (2) Solid solution. The Ti–Ag films with < 21.6 at.% Ag and the W–Ag films with < 23.9 at.% Ag exhibited solid solution structure [15]. Tungsten and silver were reported to be immiscible [27], but the energetic ion bombardment helps form such a meta-stable crystal structure during film growth. Solid solution was also reported for Mo–Ag [34] and Fe–Ag [35] films. (3) Segregation of silver nanoparticles. Ag agglomerates were observed for Nb–Ag film containing ∼ 50 at.% silver [14]. Silver nanoparticles will segregate at higher silver contents compared with those for the formation of solid solution or compounds. Segregation of silver nanoparticles was also reported for Co–Ag [36] and Ag-containing ceramic films [12, 13]. The above studies show that structure of the deposited films is generally dominated by silver content and materials nature. This finding would be useful for structure design and properties control of the metallic films containing Ag and other antibacterial agents (Cu, Mn, Zn, etc.).

Microhardness, wettability, and corrosion resistance

Microhardness of the pure W film is 2100 HV, comparable to that of W films deposited with a novel HiPIMS approach (21.3–32.2 GPa [17]), but it is higher than those of the W film deposited by magnetron sputtering (14 GPa [18]) and the

homogeneously multilayered W film fabricated by multi-step sputtering (12–13 GPa [28]). The pure W film is even harder than the DLC film (13.3 GPa [12]). Microhardness of the films is slightly reduced to 1740–1860 HV for samples S02–S08 and markedly decreased to 650 and 570 HV for samples S15 and S20, respectively (Table 1). These hardness values are much higher than those of pure Ag film (240 HV) and the stainless steel ($\sim$ 250 HV). Microhardness of the samples with $\leq$ 6.7 at.% silver is nearly seven times that of the stainless steel.

Wetting behavior of the polished and the coated stainless-steel samples was assessed by contact angle measurement (Table 3). The water contact angles are within 82°–92°. The narrow contact angle distribution indicates that W–Ag and pure Ag films do not alter hydrophobic nature of the stainless-steel substrate. The glycol contact angles are relatively lower (62°–73°). Surface free energy of the samples is determined from the water and glycol contact angles. The coated samples have higher surface energy than the polished sample, but their values (21–26 mJ/m^2) are much lower than those of the polished titanium, Ti6Al4V, and NiTi alloys (52, 41/50 and 45 mJ/m^2, respectively [37, 38]). The hydrophobic surface with low surface energy is beneficial for the biomedical applications of anti-fouling and antimicrobial materials [23, 25]. In addition, the dispersive component is the dominant for all samples. It was reported that a low polar component (or low fractional polarity) was the major parameter for good fibroblast cell proliferation [37].

Corrosion resistance of the polished and the coated stainless-steel samples was evaluated by potentiodynamic polarization test (Fig. 6). The coated samples have lower corrosion potential (E_{corr}) and larger
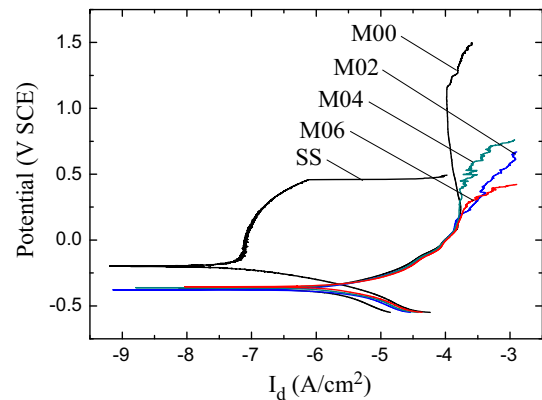
Table 3 Contact angle and surface energy of the stainless-steel samples

Samples	Contact angle (°)		Surface energy (mJ/m^2)		
	Water	Glycol	Dispersive	Polar	Sum
SS	91.1 $\pm$ 3.1	72.7 $\pm$ 0.5	13.9	6.6	20.5
M00	87.3 $\pm$ 2.1	64.7 $\pm$ 2.1	19.1	6.1	25.2
M02	82.4 $\pm$ 3.0	62.2 $\pm$ 5.2	16.0	10.0	26.0
M04	86.2 $\pm$ 3.3	64.0 $\pm$ 3.3	18.6	6.8	25.4
M06	89.7 $\pm$ 2.7	66.1 $\pm$ 7.0	20.5	4.7	25.2
MAg	91.6 $\pm$ 2.8	67.3 $\pm$ 0.8	21.5	3.7	25.2

Figure 6 Potentiodynamic polarization plots of the stainless-steel group samples.

corrosion current density (I_{corr}) values than the polished sample (Table 4). The pure tungsten-coated sample (M00) has longer passivation range and higher pitting potential than the polished sample (SS), but the passive current density (I_{pass}) of the former is nearly 1000 times larger than that of the latter. SEM observation shows that the W film underwent even corrosion during the test, although some tiny pores were formed due to the high stop potential (Fig. 7a). The W–Ag-coated samples have similar polarization plots, but their pitting potentials are much lower than that of pure W-coated sample (M00). The current peak at 0.08 V related to dissolution of silver nanoparticles found for ceramic films (DLC [12], TiO$_2$ [39], MgO [40], etc.) is absent in the plots. This indicates that silver in the W–Ag film exists in a different way (i.e., solid solution atoms) from the silver nanoparticles in the above ceramic films. The W–Ag films also exhibit the even corrosion mode (Fig. 7b, c). However, corrosion resistance (R_{corr}) is gradually decreased with the increase in silver content in the films (Table 4).

The coated stainless-steel samples were soaked in acidic PBS (pH 5.2 $\pm$ 0.1) to test their corrosion resistance at the simulated inflammatory conditions. The films were slightly corroded after 6 days of soaking, and Ag and AgCl nanocrystals (Ag 43.9 at.%, Cl 14.9 at.%) are observed at the surface of sample M06 (Fig. 7d–f). This indicates that tungsten and silver ions were released due to corrosion of the films during the soaking period. It was reported that tungsten and tungsten–DLC films were biocompatible and antibacterial [7, 20–22]. The corrosion of W–Ag films was enhanced at acidic conditions, but the

Table 4 Corrosion data of the stainless-steel group samples

Sample	E_{corr} (V SCE)	I_{corr} (μA/cm^2)	R_{corr} (Ω cm^2)	E_{pit} (V SCE)	I_{pass} (μA/cm^2)
SS	− 0.20	0.020	4.07×10^5	0.58	0.112*
M00	− 0.37	1.886	1.88×10^4	0.95	119*
M02	− 0.38	1.073	1.54×10^4	/	/
M04	− 0.36	1.080	1.34×10^4	0.23	165*
M06	− 0.35	3.948	1.02×10^4	/	/

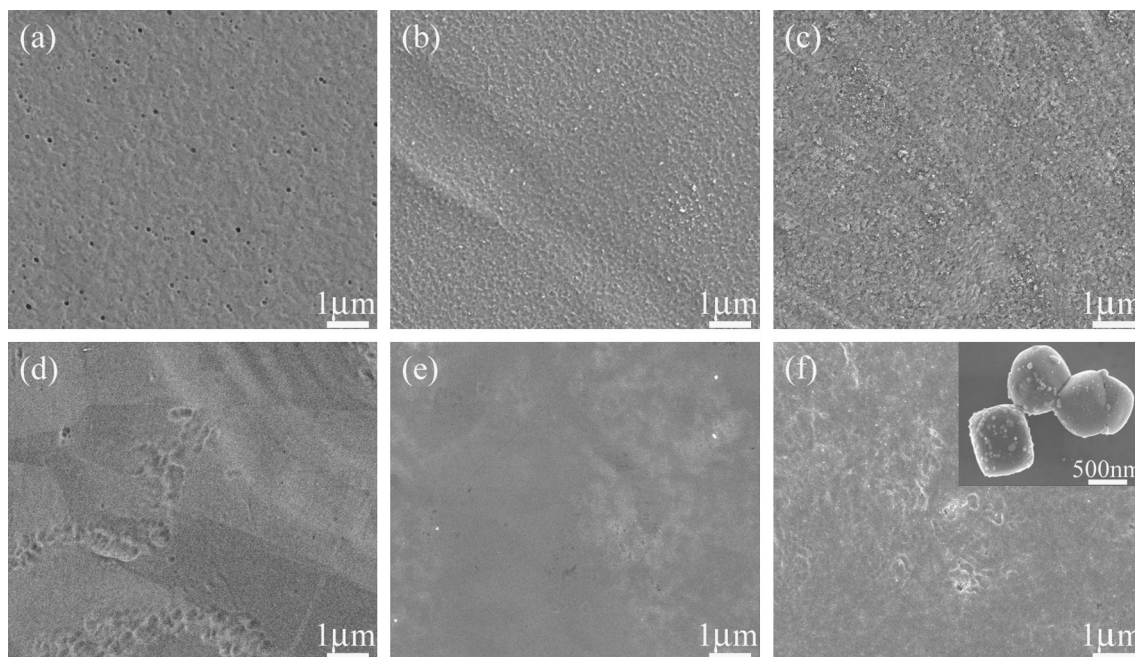*Current density at middle potential of the passivation zone

Figure 7 SEM surface images the tested stainless-steel samples: **a–c** M00, M04, M06, respectively, after electrochemical test, **d–f** M00, M04, M06, respectively, after soaking test in acid PBS.

release of tungsten and silver ions would help treat the inflammation around the films.

Antibacterial test

The antibacterial property of the stainless-steel samples was first quantitatively evaluated by agar plate counting method (Fig. 8). The polished sample SS favors bacteria growth when tested for 3 h, and the bacterial colonies are reduced when W film is coated (e.g., from 129 to 98 colonies, Fig. 9). It was reported that DLC–W film inhibited the growth of some bacteria strains, which is related to the antibacterial effect of tungsten [7]. The antibacterial ratio (AR) of samples M02, M04, M06, and MAg related to sample M00 increases with silver content of the films, being 45, 70, 91, and 100%, respectively. Thus, the W film with 4.2 at.% silver (sample M06) can obtain an AR

value of above 90%. This reveals silver-dependent antibacterial activity of the W–Ag films. To verify the antibacterial effect of W–Ag films, *E. coli* was cultured on sample M06 and stainless-steel substrate for 3 h. The SEM observation shows that the bacteria are less on sample M06, and their cell membrane is broken, and some intracellular inclusion is leaked (Fig. 10).

The content, distribution, and chemical state of sliver element play crucial roles in silver ions release and antibacterial activity of the Ag-containing films. The bactericidal mechanism of silver ions can be explained by (a) the impairing effects of silver ions on the structure and functions of bacterial cells, and (b) the reactive oxygen species (ROS) induced bacteria death, in which ROS are produced in catalysis of molecule oxygen by silver ions in water [41–43]. For metallic silver in the forms of nanoparticles or films, the nonpassive silver oxide thin film formed by
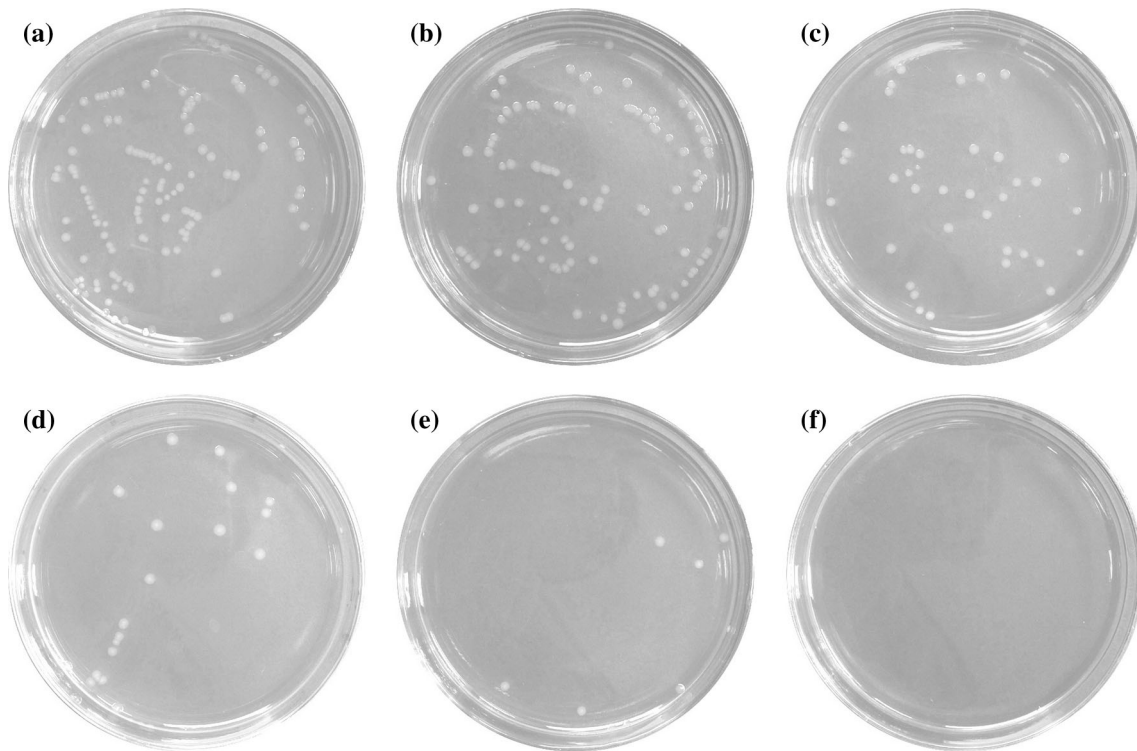
Figure 8 Typical antibacterial test results (3 h) of the stainless-steel samples by agar plate counting method: **a** SS, **b** M00, **c** M02, **d** M04, **e** M06, **f** MAg.
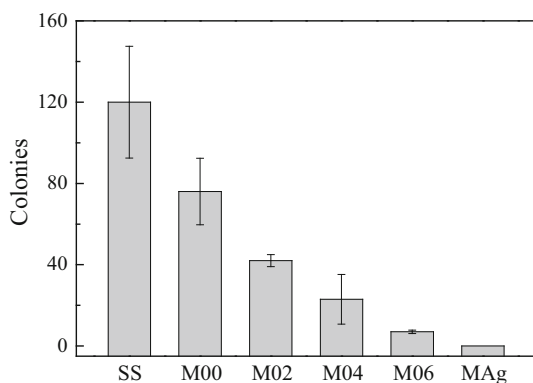

Figure 9 Bacterial colony numbers of the stainless-steel samples tested by agar plate counting method.

oxidation is essential for the release of antimicrobial Ag^+ ions in solutions [30, 31]. As for the Ag-containing metallic films with solid solution or intermetallic compound structure, the degradation of metal matrix or compound would influence the release of silver ions, as the above corrosion tests suggested.

When the samples were qualitatively tested by agar disk diffusion assay, no inhibition zone is observed for all the samples (Fig. 11). Under similar test conditions, the Ag-containing DLC [12] and TiN films deposited at 0.6 A of Ag target current showed wide inhibition zone due to silver segregation to the film surface. It was also reported that the activation of nanogalvanic couple created by embedding silver nanoparticles into carbon matrix enhanced the ionization of biocidal Ag^+ ions [11]. For W–Ag films, it seems that silver ions released from the films were limited during the test, and they can only killed bacteria that landed on the film surface. The localized antibacterial effect makes W–Ag films a useful coating to prevent bacterial adhesion or colonization. Moreover, the above tested samples were cleaned, soaked in deionized water for 2 weeks, and tested again. The AR value is still above 70% for samples M04 and M06, demonstrating their long-lasting and reusable antibacterial property due to the slow and continuous release of silver ions [29]. It was reported that DLC–Ag films with above 2 at.% silver have the improved bactericidal properties against *E. coli*, but the decreased viability of osteoblast cells [32]. The lack of silver segregation and the limited release of
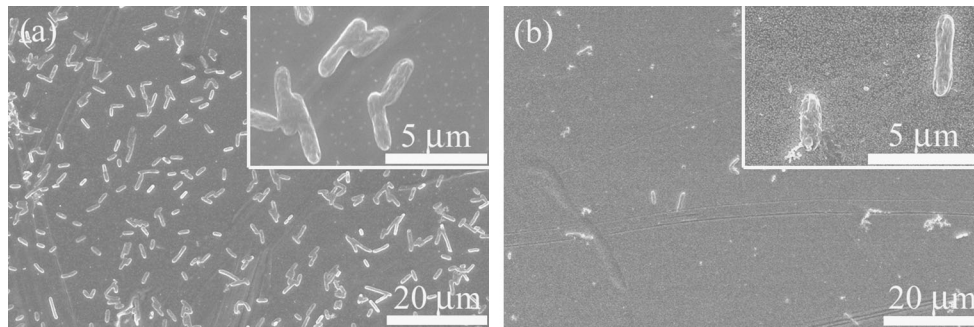
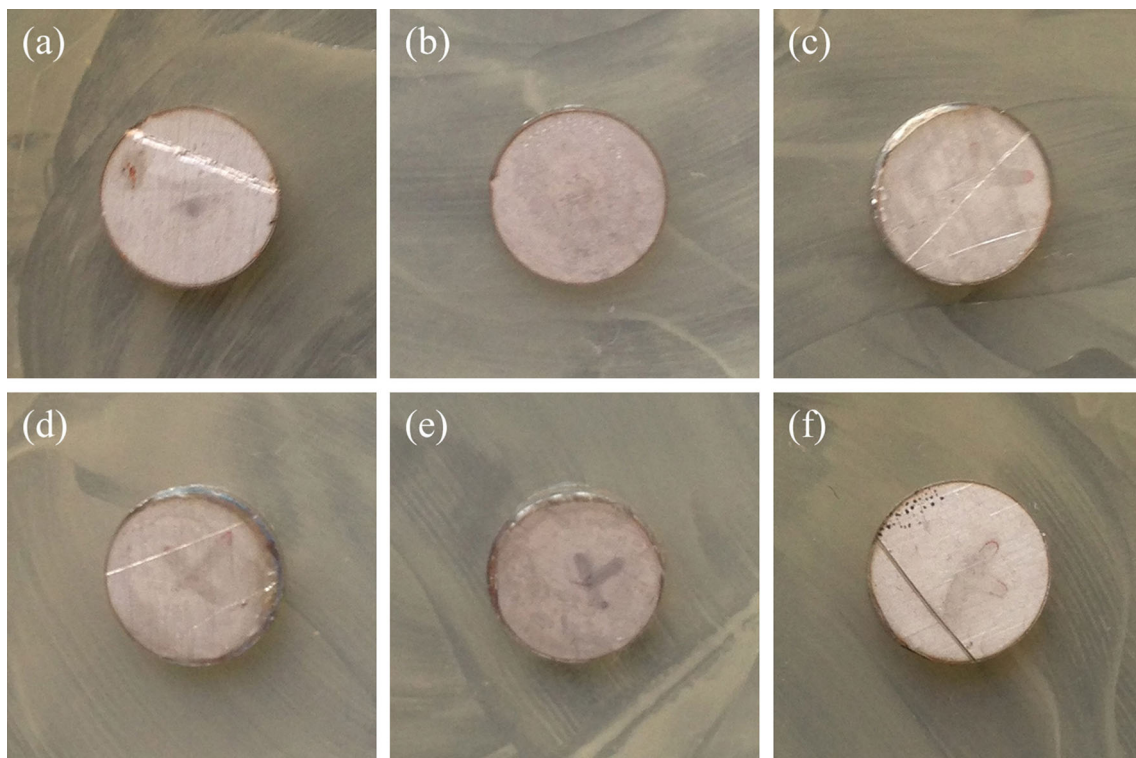**Figure 10** SEM images of the stainless-steel samples after contacted with *E. coli*: **a** SS, **b** M06.

Figure 11 Typical antibacterial test results of the stainless-steel samples (ϕ10 mm) by agar disk diffusion assay (48 h): **a** SS, **b** M00, **c** M02, **d** M04, **e** M06, **f** MAg.

silver ions would be beneficial for biocompatibility of the W–Ag films at relatively low silver content.

Conclusions

W–Ag films with silver content up to 36.2 at.% were prepared by magnetron sputtering. Adhesion of the films on glass substrate is improved by silver addition due to the reduced residual stress in the films. Silver exists in the tungsten films mainly as solid solution atoms and silver segregation at the film surface is not obvious. Tungsten is slightly oxidized (WO_3) at the top surface of the film, and silver presents mainly in metallic state.

W–Ag films with ≤ 6.7 at.% silver are nearly seven times as hard as that of the stainless-steel substrate. W–Ag and pure Ag films do not alter hydrophobic nature of stainless steel. The corrosion tests reveal even corrosion of the films and the corrosion resistance is decreased by silver addition. The

antibacterial property of W–Ag films is tungsten related, silver dependent, localized, long-lasting, and reusable.

Compliance with ethical standards

Conflict of interest The authors declare that they have no conflict of interest.

References

[1] Gould IM (2006) Costs of hospital-acquired methicillin-resistant Staphylococcus aureus (MRSA) and its control. Int J Antimicrob Agents 28:379–384

[2] Dong Y, Li X, Tian L, Bell T, Sammons RL, Dong H (2011) Towards long-lasting antibacterial stainless steel surfaces by combining double glow plasma silvering with active screen plasma nitriding. Acta Biomater 7:447–457

[3] Kawakami H, Yoshida K, Nishida Y, Kikuchi Y, Sato Y (2008) Antibacterial properties of metallic elements for alloying evaluated with application of JIS Z 2801:2000. ISIJ Int 48:1299–1304

[4] Mihailescu IN, Bociaga D, Socol G, Stan GE, Chifiriuc M-C, Bleotu C, Husanu MA, Popescu-Pelin G, Duta L, Luculescu CR, Negut I, Hapenciuc C, Besleaga C, Zgura I, Miculescu F (2016) Fabrication of antimicrobial silver-doped carbon structures by combinatorial pulsed laser deposition. Int J Pharm 515:592–606

[5] Raucci MG, Adesanya K, Di Silvio L, Catauro M, Ambrosio L (2010) The biocompatibility of silver-containing Na$_2$O·CaO·2SiO$_2$ glass prepared by sol-gel method: In vitro studies. J Biomed Mater Res Part B 92B:102–110

[6] Bellantone M, Williams HD, Hench LL (2002) Broad-spectrum bactericidal activity of Ag$_2$O-doped bioactive glass. Antimicrob Agents Chemother 46:1940–1945

[7] Cazalini EM, Miyakawa W, Teodoro GR, Sobrinho ASS, Matieli JE, Massi M, Koga-Ito CY (2017) Antimicrobial and anti-biofilm properties of polypropylene meshes coated with metal-containing DLC thin films. J Mater Sci Mater Med 28:97

[8] Chang Y-Y, Huang H-L, Chen Y-C, Weng J-C, Lai C-H (2013) Characterization and antibacterial performance of ZrNO–Ag coatings. Surf Coat Technol 231:224–228

[9] Hsieh JH, Yeh TH, Li C, Chang SY, Chiu CH, Huang CT (2013) Mechanical properties and antibacterial behaviors of TaN-(Ag,Cu) nanocomposite thin films after annealing. Surf Coat Technol 228:S116–S119

[10] Xu R, Yang X, Jiang J, Li P, Zhang X, Wu G, Chu PK (2015) Effects of silver plasma immersion ion implantation on the surface characteristics and cytocompatibility of titanium nitride films. Surf Coat Technol 279:166–170

[11] Manninen NK, Calderon S, Carvalho I, Henriques M, Cavaleiro A, Carvalho S (2016) Antibacterial Ag/a-C nanocomposite coatings: the influence of nano-galvanic a-C and Ag couples on Ag ionization rates. Appl Surf Sci 377:283–291

[12] Wang LJ, Zhang F, Fong A, Lai KM, Shum PW, Zhou ZF, Gao ZF, Fu T (2018) Effects of silver segregation on sputter deposited antibacterial silver-containing diamond-like carbon films. Thin Solid Films 650:58–64

[13] Calderon Velasco S, Cavaleiro A, Carvalho S (2016) Functional properties of ceramic-Ag nanocomposite coatings produced by magnetron sputtering. Prog Mater Sci 84:158–191

[14] Wojcieszak D, Mazur M, Kaczmarek D, Mazur P, Szponar B, Domaradzki J, Kepinski L (2016) Influence of the surface properties on bactericidal and fungicidal activity of magnetron sputtered Ti–Ag and Nb–Ag thin films. Mater Sci Eng C 62:86–95

[15] Bai L, Hang R, Gao A, Zhang X, Huang X, Wang Y, Tang B, Zhao L, Chu PK (2015) Nanostructured titanium–silver coatings with good antibacterial activity and cytocompatibility fabricated by one-step magnetron sputtering. Appl Surf Sci 355:32–44

[16] Lopes C, Goncalves C, Borges J, Polcar T, Rodrigues MS, Barradas NP, Alves E, Le Bourhis E, Couto FM, Macedo F, Fonseca C, Vaz F (2015) Evolution of the functional properties of titanium-silver thin films for biomedical applications: influence of in-vacuum annealing. Surf Coat Technol 261:262–271

[17] Velicu I-L, Tiron V, Porosnicu C, Burducea I, Lupu N, Stoian G, Popa G, Munteanu D (2017) Enhanced properties of tungsten thin films deposited with a novel HiPIMS approach. Appl Surf Sci 424:397–406

[18] Yang L, Zhang K, Wen M, Hou ZP, Gong C, Liu XC, Hu CQ, Cui XQ, Zheng WT (2017) Highly hard yet toughened bcc-W coating by doping unexpectedly low B content. Sci Rep 7:9353

[19] Fu T, Zhou ZF, Li KY, Shen YG (2005) Characterization of sputter deposited W–Si–N coatings based on α-W structure. Mater Lett 59:618–623

[20] Li H, Zheng Y, Pei YT, De Hosson JTM (2014) TiNi shape memory alloy coated with tungsten: a novel approach for biomedical applications. J Mater Sci Mater Med 25:1249–1255

[21] Antunes RA, de Lima NB, Rizzutto MdA, Higa OZ, Saiki M, Costa I (2013) Surface interactions of a W-DLC-coated biomedical AISI 316L stainless steel in physiological solution. J Mater Sci Mater Med 24:863–876

[22] Mansano RD, Ruas R, Mousinho AP, Zambom LS, Pinto TJA, Amoedo LH, Massi M (2008) Use of diamond-like carbon with tungsten (W-DLC) films as biocompatible material. Surf Coat Technol 202:2813–2816

[23] Swiatek L, Olejnik A, Grabarczyk J, Jedrzejczak A, Sobczyk-Guzenda A, Kaminska M, Jakubowski W, Szymanski W, Bociaga D (2016) Multi-doped diamond like-carbon coatings (DLC-Si/Ag) for biomedical applications fabricated using the modified chemical vapour deposition method. Diam Relat Mater 67:54–62

[24] Handzlik P, Fitzner K (2013) Corrosion resistance of Ti and Ti–Pd alloy in phosphate buffered saline solutions with and without H_2O_2 addition. Trans Nonferrous Met Soc China 23:866–875

[25] Lan W-C, Ou S-F, Lin M-H, Ou K-L, Tsai M-Y (2013) Development of silver-containing diamond-like carbon for biomedical applications. Part I: microstructure characteristics, mechanical properties and antibacterial mechanisms. Ceram Int 39:4099–4104

[26] Baba K, Hatada R, Flege S, Ensinger W, Shibata Y, Nakashima J, Sawase T, Morimura T (2013) Preparation and antibacterial properties of Ag-containing diamond-like carbon films prepared by a combination of magnetron sputtering and plasma source ion implantation. Vacuum 89:179–184

[27] Wen SP, Guo JG (2013) Development of arrayed nanoporous Ag/W films by alternate deposition. Mater Technol 28:165–168

[28] Peng MJ, Yang JJ, Zhang FF, Lu CY, Wang LM, Liao JL, Yang YY, Liu N (2017) Improved irradiation tolerance of W thin films with homogeneously multilayered structure. Surf Coat Technol 313:230–235

[29] Cloutier M, Tolouei R, Lesage O, Levesque L, Turgeon S, Tatoulian M, Mantovani D (2014) On the long term antibacterial features of silver-doped diamondlike carbon coatings deposited via a hybrid plasma process. Biointerphases 9:029013

[30] Rebelo R, Calderon SV, Fangueiro R, Henriques M, Carvalho S (2016) Influence of oxygen content on the antibacterial effect of Ag–O coatings deposited by magnetron sputtering. Surf Coat Technol 305:1–10

[31] Ferreri I, Calderon SV, Escobar Galindo R, Palacio C, Henriques M, Piedade AP, Carvalho S (2015) Silver activation on thin films of Ag–ZrCN coatings for antimicrobial activity. Mater Sci Eng C 55:547–555

[32] Bociaga D, Jakubowski W, Komorowski P, Sobczyk-Guzenda A, Jedrzejczak A, Batory D, Olejnik A (2016) Surface characterization and biological evaluation of silver-incorporated DLC coatings fabricated by hybrid RF PACVD/MS method. Mater Sci Eng C 63:462–474

[33] Cloutier M, Turgeon S, Busby Y, Tatoulian M, Pireaux JJ, Mantovani D (2016) Controlled distribution and clustering of silver in Ag-DLC nanocomposite coatings using a hybrid plasma approach. ACS Appl Mater Interfaces 8:21020–21027

[34] Tung SC, Cheng YT (1993) Microstructures and tribological characteristics of electron-beam co-deposited Ag/Mo thin-film coatings. Wear 162:763–772

[35] Tamisari M, Spizzo F, Sacerdoti M, Battaglin G, Ronconi F (2011) Correlation between structural and giant magnetoresistance properties of Fe–Ag nanogranular films. J Nanopart Res 13:5203–5210

[36] Takahashi M, Notohara Y, Sunakawa Y, Ishio S (1985) Magnetic properties of Co/Cr and Co/Ag layered films. IEEE Transl J Magn Jpn 1:829–830

[37] Ponsonnet L, Reybier K, Jaffrezic N, Comte V, Lagneau C, Lissac M, Martelet C (2003) Relationship between surface properties (roughness, wettability) of titanium and titanium alloys and cell behaviour. Mater Sci Eng C 23:551–560

[38] Echeverry-Rendon M, Galvis O, Aguirre R, Robledo S, Guillermo Castano J, Echeverria F (2017) Modification of titanium alloys surface properties by plasma electrolytic oxidation (PEO) and influence on biological response. J Mater Sci Mater Med 28:169

[39] Fu T, Shen YG, Alajmi Z, Yang SY, Sun JM, Zhang HM (2015) Sol–gel preparation and properties of Ag–TiO_2 films on surface roughened Ti–6Al–4V alloy. Mater Sci Technol 31:501–505

[40] Alajmi Z, Fu T, Zhao YT, Yang SY, Sun JM (2016) Ag-enhanced antibacterial property of MgO film. Mater Sci Forum 859:90–95

[41] Loza K, Diendorf J, Sengstock C, Ruiz-Gonzalez L, Gonzalez-Calbet JM, Vallet-Regi M, Koller M, Epple M (2014) The dissolution and biological effects of silver nanoparticles in biological media. J Mater Chem B 2:1634–1643

[42] Li W-R, Xie X-B, Shi Q-S, Zeng H-Y, Ou-Yang Y-S, Chen Y-B (2010) Antibacterial activity and mechanism of silver nanoparticles on *Escherichia coli*. Appl Microbiol Biotechnol 85:1115–1122

[43] Shrivastava S, Bera T, Roy A, Singh G, Ramachandrarao P, Dash D (2007) Characterization of enhanced antibacterial effects of novel silver nanoparticles. Nanotechnology 18:225103